Intramultiplet mixing in collisions of calcium $4s\,4p\ ^3P_J^o$ with helium: Measurement of state-to-state cross sections

H.-J. Yuh and P. J. Dagdigian
Department of Chemistry, Johns Hopkins University, Baltimore, Maryland 21218
(Received 17 January 1983)

An optical-pumping state-selection technique for the study of collisions of ^3P atoms in individual spin-orbit states is described. This technique is used to determine state-to-state intramultiplet-mixing cross sections for collisions of Ca $^3P^o$ with helium in a beam–static-gas arrangement. The derived cross sections are as follows: for $J=2\rightarrow J'=1$, 31.9 ± 4.2 Å^2; for $J=2\rightarrow J'=0$, 5.5 ± 1.6 Å^2; and for $J=1\rightarrow J'=0$, 2.0 ± 5.0 Å^2. These quantities represent averages over the translational-energy distribution (average energy 0.0556 eV). In the following paper Alexander, Orlikowski, and Straub present quantum close-coupling cross sections as a function of translational energy, using the pseudopotential Ca-He interaction curves of Malvern [J. Phys. B 11, 831 (1978)]. The experimental $2\rightarrow1$ and $2\rightarrow0$ cross sections are found to be 3 to 4 times larger than the calculated theoretical values. In contrast to the theoretical prediction for the ratio of the smaller cross sections, the $2\rightarrow0$ cross section is found to be larger than the $1\rightarrow0$ cross section.

I. INTRODUCTION

There has been much theoretical and experimental work on collisional intramultiplet mixing in ^2P atoms, particularly in the alkali metals.[1–9] The collisions of alkali metals with noble gases are among the simplest inelastic processes which can occur in atomic collisions. The cross sections have been found to be appreciable, but decrease sharply with increasing spin-orbit splitting. The mechanisms responsible for these fine-structure–changing transitions have been intensively investigated.[1] On the contrary, there has been much less study of collisional mixing of spin-orbit states in triplet-state atomic systems. In the latter, three distinct fine-structure–changing transitions will occur as compared to the one transition which describes a ^2P system.

There have been some experimental studies on intramultiplet mixing in ^3P states of heavy metal atoms, such as Hg and Cd.[10–19] These states have large spin-orbit splittings, and the inelastic cross sections were found to be very small for collisions with noble gases.[10,11] The mixing cross sections are enhanced if the collision partner is a molecule,[12–18] as with alkali metals.[3–5,7–9] However, the involvement of possible near-resonant [electronic-to-vibrational (E-V) or electronic-to-rotational (E-R)] mechanisms[16,17] and competition with other channels,[20–23] such as quenching and chemical reaction, complicates experimental and theoretical study of these systems. In addition, *ab initio* computation of the relevant potential-energy curves is very difficult for heavy metal atoms, even for interaction with the noble gases.

We have become interested in collisional intramultiplet mixing in the group-II A metals since they have metastable $^3P_J^o$ states which are more suitable for detailed study. The smaller spin-orbit splittings imply larger-mixing cross sections in collisions with noble gases. Indeed, such collisions have been found to equilibrate thermally the $^3P_J^o$ multiplet on a time scale short compared to the $^3P_1^o$ radiative lifetime for Mg, Ca, and Sr.[24–26] In the present work, we present an experimental study of collisions of Ca $4s\,4p\ ^3P_J^o$ atoms with helium in which state-to-state intramultiplet-mixing cross sections have been determined:

$$\mathrm{Ca}(^3P_J)+\mathrm{He}\rightleftarrows\mathrm{Ca}(^3P_{J'}^o)+\mathrm{He}\ . \tag{1}$$

The $J=1$ and 2 spin-orbit states lie 52.2 and 158.0 cm^{-1}, respectively, above the $J=0$ state in this multiplet. In the accompanying paper, Alexander, Orlikowski, and Straub[27] present the formalism for quantum studies of the scattering of $^3P_J^o$ atoms with a structureless partner and use this theoretical apparatus to compute intramultiplet cross sections for Ca($^3P_J^o$)-He collisions, for which potential curves from a pseudopotential calculation are available.[28]

The organization of the present paper is as follows. In Sec. II, our experimental apparatus and procedure are discussed, in particular the J-state selection technique, which is achieved by optical pumping[29–32] with a single-mode cw dye laser on a $4s\,5s\ ^3S_1\leftarrow4s\,4p\ ^3P_J^o$ line. The present optical-pumping scheme differs from those employed previously in scattering studies[32] in that the excited states radiate back to the states of interest and not to collisionally disconnected states. In Appendix A, we show that no coherences are generated in the present arrangement. In Sec. III, we present the $^3P_J^o$ populations as a function of He scattering gas pressure when each of the three $^3P_J^o$ states is optically pumped in turn; the populations are determined by laser fluorescence detection with a second dye laser. We derive in Appendix B the appropriate intensity factors relating fluorescence intensities to populations. The experimental data are used in Sec. IV to derive state-to-state cross sections. Finally, our results are discussed in Sec. V and, in particular, compared with the theoretical results obtained in the accompanying paper.

II. EXPERIMENTAL ARRANGEMENT

Figure 1 presents a schematic diagram of the experimental arrangement. A near-effusive beam of electronically excited metastable Ca atoms ($4s\,4p\ ^3P_J^o$ and $4s\,3d\ ^1D$) was generated in a discharge source which has been described in detail previously.[33] The typical source operat-

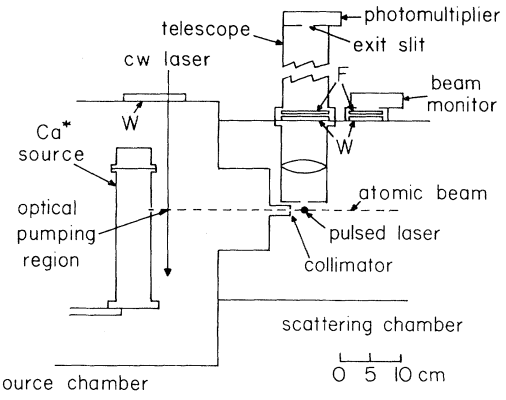

FIG. 1. Schematic drawing of the experimental apparatus. W and F denote a window and an interference filter, respectively.

ing temperature was approximately 1335 K with the discharge voltage below 9 V and current at 1—1.5 A. Under these conditions, the ^1D to $^3P_J^o$ population ratio was approximately 3.5%.[33] The $^3P_1^o$ population was monitored in the scattering chamber by observing the $4s\,4p\,^3P_1^o \rightarrow 4s^2\,^1S$ emission line at 657.3 nm with a photometer [photomultiplier with interference filter centered at 650 nm, full width at half maximum (FWHM) 50 nm].

Directly in front of the source, the metastable atomic beam was crossed with a single-mode cw dye laser (Coherent CR599-21 with rhodamine 6G dye); the laser beam power and cross-sectional area at the interaction zone were 40—70 mW and 0.7 cm^2, respectively. The dye laser was tuned to one of the $4s\,5s\,^3S_1 \leftarrow 4s\,4p\,^3P_J^0$ lines near 610 nm in order to deplete one of the $^3P_J^o$ states by optical pumping.[29—32] The laser wavelength was first adjusted to within 0.001 nm of a line with a fringe-counting interferometer by comparison with an unstabilized He-Ne laser.[34] It was then located accurately on line center by observing the decrease or increase in the $^3P_1^o$ beam monitor, depending on whether the $^3P_1^o$ or $^3P_{0\text{ or }2}^o$ levels were being depleted.

The atomic beam passed through a collimator (0.32×0.64 cm^2) 24.1 cm downstream of the optical pumping region and entered the scattering chamber, to which helium target gas could be introduced through a needle valve. During a run, the diffusion pump for this chamber was choked by nearly completely closing its gate valve. Pressures of 2.5 mTorr or less, measured with a capacitance manometer (Datametrics 1173 with 1 Torr head), were employed. Its accuracy was checked by comparison with a second capacitance manometer (MKS 310BHS-1 head and 170M gauge), for which the manufacturer's stated accuracy in this pressure range is ±1%. In making this comparison, account was taken of the thermal transpiration effect (4±1%) due to heating of the sensor. We estimate the uncertainty in our pressure measurements to be ±5%, due mainly to pressure drifts and fluctuations. The pressure in the source chamber never exceeded 3×10^{-5} Torr during an experiment.

The relative populations of the three $^3P_J^o$ levels were determined in the scattering chamber a distance $l=1.27\pm0.1$ cm downstream of the collimator by laser fluorescence detection employing the $4s\,5s\,^3S_1 \leftarrow 4s\,4p\,^3P_J^o$ multiplet. A nitrogen-laser-pumped tunable dye laser (diameter 0.4 cm at the excitation zone) was used; this system has been described in detail previously.[35] In the current study, fluorescence was detected through a telescope with a Hamamatsu R928 photomultiplier through a narrow-band (10 nm FWHM) filter in order to block the intense background light, expecially $^3P_1 \rightarrow {}^1S$ emission from the beam. Through a series of baffles on the laser entrance and exit port, as well as by the spatial filtering provided by the telescope, scattered laser light was entirely negligible.

Simultaneous measurements of the laser pulse energy were also made, and the fluorescence signal was normalized to constant energy. It was found that the pulse-to-pulse fluctuation of the fluorescence signals was considerably in excess of that of the laser pulse energy variations. This was the principal factor determining the accuracy with which the $^3P_J^o$ populations could be measured. Since the atomic absorption line profiles are considerably narrower than the ~0.7 cm^{-1} bandwidth of the pulsed dye laser, variations of its frequency profile from pulse to pulse can cause such fluctuations.

Two types of laser fluorescence measurements were carried out. In the first, the relative populations of the $^3P_J^o$ levels at constant scattering gas pressure (usually zero) were determined by comparing the laser fluorescence signals of each $4s\,5s\,^3S_1 \leftarrow 4s\,4p\,^3P_J^o$ line. For this, the pulsed dye laser was attenuated so that the fluorescence signals were linear with laser power. In the second type of study, the pressure variation of each $^3P_J^o$ population was determined from the variation of the fluorescence intensity of the appropriate line at constant laser power. The laser intensity was also attenuated in order to avoid optical pumping effects.

III. OBSERVATIONS

Figure 2 displays the changes induced in the $^3P_1^o \rightarrow {}^1S$ beam monitor signal as the cw dye laser was tuned over each $^3S_1 \leftarrow {}^3P_J^o$ line. It is clear from Fig. 2(c) that the optical pumping process removes most of the $^3P_1^o$ population when the laser is coincident with the $^3S_1 \leftarrow {}^3P_1^o$ line. Since the $4s\,5s\,^3S_1$ state decays radiatively only to the $4s\,4p\,^3P_J^o$ multiplet, the $^3P_1^o$ population is increased when the laser is tuned to the other lines of the $^3S_1 \leftarrow {}^3P_J^o$ multiplet, as Figs. 2(a) and 2(b) show. The linewidths in Fig. 2 are considerably in excess of the natural linewidth and residual Doppler width and arise mainly from power broadening. There is no hyperfine structure for any of the naturally occurring Ca isotopes of significant abundance.

In fact, Fig. 2 underestimates the efficiency of the optical-pumping state-selection process, since a somewhat larger collimator was employed than in the scattering experiments. Laser fluorescence detection with the second dye laser showed almost complete depletion ($\lesssim$2% left) at power densities of ~50 mW/cm^2, with corresponding increases in the densities of the other $^3P_J^o$ states, when the 0.32×0.64 cm^2 collimator was used.

The present experiment differs from those of Bergmann *et al.*[32] on Na_2 in that in the latter study only a negligible fraction of the excited molecules radiate back into the lev-

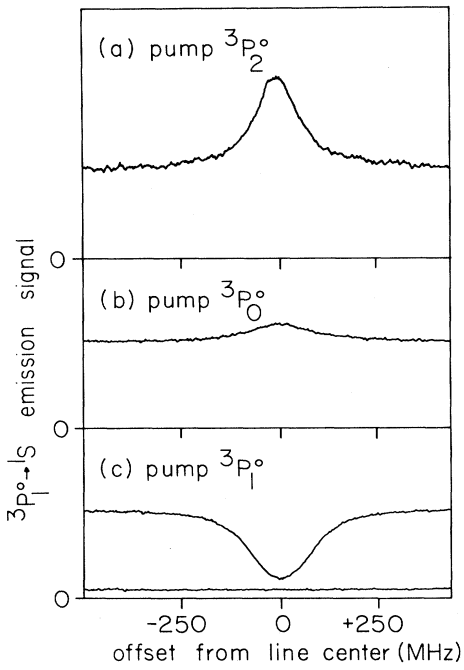

FIG. 2. Change in the $^3P_1 \rightarrow {}^1S$ beam monitor signal as the cw pump laser is scanned across the (a) $^3S_1 \leftarrow {}^3P^o_2$ line at 616.217 nm, (b) $^3S_1 \leftarrow {}^3P^o_0$ line at 610.272 nm, and (c) $^3S_1 \leftarrow {}^3P^o_1$ line at 612.222 nm. In (c), the background level when the source discharge is turned off (hence, no production of $^3P^o_J$ atoms) is indicated. For all these scans, He was absent from the scattering chamber.

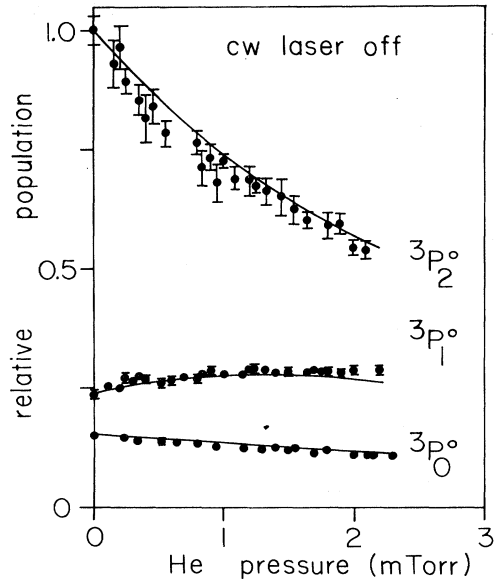

FIG. 3. Variation of the $^3P^o_J$ populations, as determined by laser fluorescence measurements, vs He scattering gas pressure, with no optical-pumping state selection. The data have been normalized so that the $^3P^o_2$ population is unity at zero pressure; error bars are ± one standard deviation. Solid lines are best fits using Eqs. (2)—(4) and the cross sections reported in Table I.

els of interest. Since optically pumped atoms decay, in part, into the unpumped $^3P^o_J$ states and since coherences are known to be generated in various optical-pumping experiments,[36–38] it is important to understand quantitatively our optical-pumping state-selection technique. The existence of coherences would significantly complicate the interpretation of our scattering experiments. In Appendix A, we present a density-matrix calculation of our experiment. We conclude that there are no coherences present in the unpumped $^3P^o_J$ states and, moreover, that the M_J distributions are nearly isotropic. The mixing due to the earth's magnetic field and the beam-velocity averaging are crucial in eliminating the coherences. In Appendix B, the line-strength factors appropriate to laser fluorescence detection employing the $^3S \leftarrow {}^3P^o_J$ multiplet are derived.

In the scattering experiments, the $^3P^o_J$ populations were determined in the scattering chamber as a function of helium target pressure. Figure 3 presents the relative populations of the spin-orbit levels with the cw pump laser off, and hence all three $^3P^o_J$ levels present initially. It is obvious that elastic scattering out of the field of view of the detector is occurring since the total population, summed over all the spin-orbit levels, decreases as the He pressure is increased; the $^3P^o$ to ^1S electronic quenching cross section is known[39] to be very small. More interesting is the observation that the J-state distribution changes as a function of pressure. In particular, the $^3P^o_1$ population actually increases slightly, in contrast to that of the other levels. Because of the large initial $^3P^o_2$ population, this increase is most likely due to $J=2 \rightarrow J'=1$ intramultiplet mixing.

Figures 4—6 display the results when the $^3P^o_2$, $^3P^o_1$, and $^3P^o_0$ levels, respectively, are depleted. The populations of the initially depleted levels are observed to grow with in-

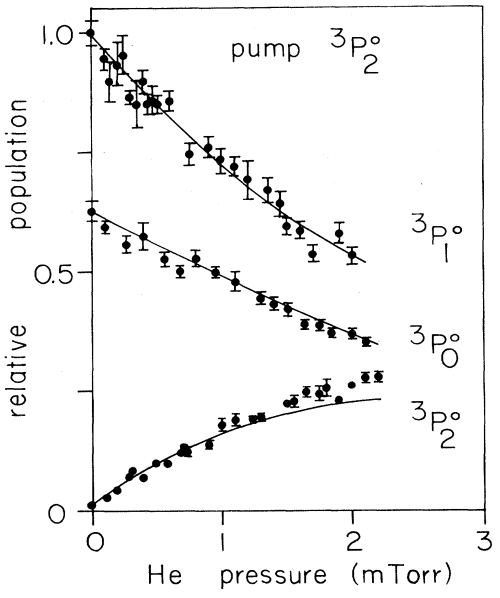

FIG. 4. Variation of the $^3P^o_J$ populations vs He scattering gas pressure, with the $^3P^o_2$ level depleted. The data have been normalized so that the $^3P^o_1$ population is unity at zero pressure; error bars are ± one standard deviation. Solid lines are best fits using Eqs. (2)—(4) and the cross sections reported in Table I.

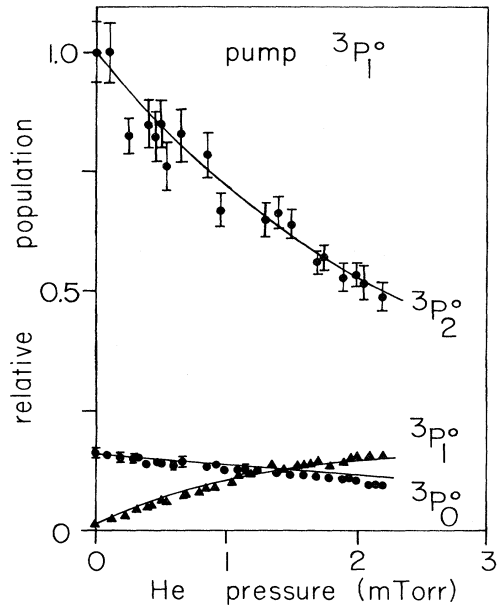

FIG. 5. Variation of the $^3P_J^o$ populations vs He scattering gas pressure, with the $^3P_1^o$ level depleted. The data have been normalized so that the $^3P_2^o$ population is unity at zero pressure; error bars are ± one standard deviation. Solid lines are best fits using Eqs. (2)—(4) and the cross sections reported in Table I.

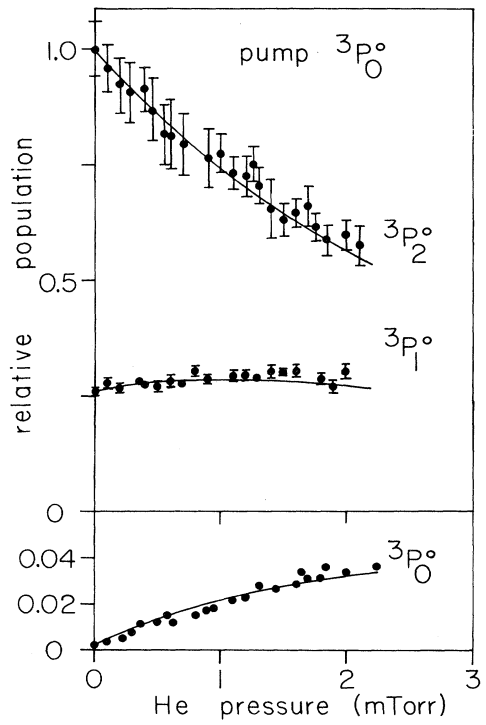

FIG. 6. Variation of the $^3P_J^o$ populations vs He scattering gas pressure, with the $^3P_0^o$ level depleted. The data have been normalized so that the $^3P_2^o$ population is unity at zero pressure; error bars are ± one standard deviation. Solid lines are best fits using Eqs. (2)—(4) and the cross sections reported in Table I.

creasing He pressure. This is obviously the result of collisional fine-structure-changing transitions. The initial rate of growth is large for $^3P_2^o$ and $^3P_1^o$ in Figs. 4 and 5, respectively, which is consistent with the large magnitude of the $J=2 \rightleftarrows J'=1$ cross sections deduced from the data in Fig. 3. By microscopic reversibility,[40] the forward and reverse cross sections should be of comparable magnitude since the translational energy is much greater than the internal energy difference with the reverse rate being slightly larger because of a larger degeneracy factor. This latter observation explains why the initial increase for $^3P_2^o$ in Fig. 4 is slightly greater than that for $^3P_1^o$ in Fig. 5. By contrast, the initial rate of growth of the $^3P_0^o$ population in Fig. 6 is very much smaller. This suggests that the $J=1 \rightleftarrows J'=0$ and $J=2 \rightleftarrows J'=0$ cross sections are much smaller in magnitude. In the next section, we quantify the observations by fitting these data to a kinetic model.

IV. DETERMINATION OF CROSS SECTIONS

In the kinetic modeling of the He pressure dependence of the $^3P_J^o$ populations, it is necessary to consider only collisional intramultiplet mixing and beam attenuation (elastic scattering out of the detector field of view). The $^3P^o \rightarrow {}^1S$ He quenching cross section has been previously determined[39] to be very small (8.9×10^{-5} Å^2). Also, because of the small concentration of the higher-lying Ca(^1D) state, collisional transfer and radiative decay[41] from ^1D to $^3P_J^o$ can be ignored. Thus, the rate equations governing the populations n_J of the $^3P_J^o$ levels versus He scattering gas density n are

$$\frac{dn_0}{dt}=-(k_{0\rightarrow1}+k_{0\rightarrow2}+k_e)nn_0+k_{1\rightarrow0}nn_1+k_{2\rightarrow0}nn_2\ , \tag{2}$$

$$\frac{dn_1}{dt}=k_{0\rightarrow1}nn_0-[k_r+(k_{1\rightarrow2}+k_{1\rightarrow0}+k_e)n]n_1 +k_{2\rightarrow1}nn_2\ , \tag{3}$$

$$\frac{dn_2}{dt}=k_{0\rightarrow2}nn_0+k_{1\rightarrow2}nn_1-(k_{2\rightarrow0}+k_{2\rightarrow1}+k_e)nn_2\ . \tag{4}$$

Here $k_{J\rightarrow J'}=\langle v\sigma_{J\rightarrow J'}\rangle$ is the rate constant for collisional transfer from the $^3P_J^o$ to the $^3P_{J'}^o$ level, $k_e=\langle v\sigma_e^{\rm eff}\rangle$ is the rate constant for elastic scattering beyond the detector field of view, and $k_r=(2.00\pm0.16)\times10^3$ s^{-1} is the $^3P_1^o \rightarrow {}^1S$ radiative decay rate.[24,42,43] The bimolecular rate constants can be related[27] to velocity-averaged cross sections $\bar{\sigma}$ by dividing by the average relative velocity $\bar{v}$. Expressions for the n_J populations versus n at a fixed scattering path length l were obtained using Laplace transforms.[44] These formulas were checked with results obtained by numerically integrating Eqs. (2)—(4).

The collisional rate constants in Eqs. (2)—(4) were deter-

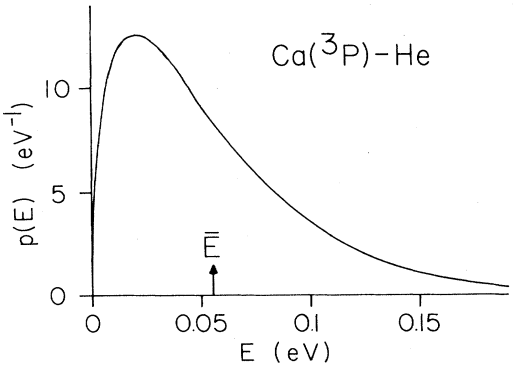

FIG. 7. Calculated translational energy distribution for the $Ca(^3P^o)$-He collisions in the beam-gas arrangement. The $Ca(^3P^o)$ velocity distribution was taken from Ref. 33. The average energy $\bar{E}$ is indicated.

mined by fitting the data in Figs. 3—6 to these equations. To reduce the number of parameters, the ratios of forward and reverse rates were fixed by detailed balance[40]:

$$k_{J\to J'}/k_{J'\to J}=[(2J'+1)/(2J+1)]e^{-\Delta E/k_B T_{\text{eff}}}, \quad (5)$$

where

$$\Delta E = E(^3P^o_{J'}) - E(^3P^o_J)$$

is the forward exoergicity and T_{eff} is the translational temperature. Even though Eq. (5) applies rigorously only to a Maxwellian velocity distribution, we have utilized this relation here by setting T_{eff} equal to $2\bar{E}/3k_B$, where $\bar{E}$ is the average relative translational energy. The latter is calculated[45,46] to be 0.0556 ± 0.0015 eV, by convolution of the He Maxwellian distribution with a previously determined[33] $Ca(^3P^o)$ beam-velocity distribution. The uncertainty is derived from a possible $\pm10\%$ variation in the latter. The calculated $Ca(^3P^o)$-He relative—translational-energy distribution is displayed in Fig. 7. This is almost identical to that of a Boltzmann distribution with T_{eff} appropriate to our experiment (430 ± 10 K). Because the energy spacings are smaller than $k_B T_{\text{eff}}$, the uncertainty in T_{eff} does not significantly affect the ratios in Eq. (5). These are calculated to be 1.17 ± 0.01 for $J=1,J'=2$; 2.95 ± 0.04 for $J=0,J'=2$; and 2.52 ± 0.01 for $J=0,J'=1$.

With the application of Eq. (5), there are only four rate constants $(k_e,k_{1\to0},k_{2\to0},k_{2\to1})$ which are needed to fit the experimental data. A nonlinear least-squares procedure[47] was used to determine these parameters. Each experimental point in Figs. 3—6 was weighted by the inverse square of its standard deviation (error bars indicated on the figures), and the parameters adjusted to minimize the reduced χ^2.[47] This weighting procedure emphasizes the collisional repopulation of the depleted levels since the standard deviations for these data were the smallest in size. The magnitude of this repopulation process is most important in determining the inelastic rate constants. Table I presents the best-fit velocity-averaged cross sections $\bar{\sigma}$, obtained by dividing the derived rate constants by the average relative velocity $\bar{v}=1.59\times10^5$ cm/sec for $Ca(^3P^o)$-He intramultiplet mixing and elastic beam attenuation. The 1σ error estimates were obtained by the procedure of Bevington,[47] wherein the standard deviation of a parameter was equated with the variation required to increase the reduced χ^2 by unity with the other parameters reoptimized. Also included in the error estimates are the uncertainties in the pressure and path length measurements.

As anticipated by the discussion in Sec. III, the $2\to1$ cross section is found to be the largest of the inelastic cross sections and is the most precisely determined. Because of the presence at zero pressure of two spin-orbit states, our experimental data fix the smaller $2\to0$ and $1\to0$ cross sections much less well. The repopulation of the depleted $^3P^o_0$ level in Fig. 6 fixes the weighted sum of these cross sections, while the small effects of these cross sections on the repopulation of the depleted $^3P_2$ and $^3P_1$ levels in Figs. 4 and 5, respectively [e.g., $J=0\to J'=2$ and $J=0\to J'=1$], must be ascertained to fix these cross sections individually. It can be seen from Table I that the $2\to0$ cross section is better determined than the $1\to0$ value. This is due, in part, to the much larger initial $^3P^o_2$ population over that of $^3P^o_1$ when the $^3P^o_0$ level is depleted (Fig. 6). In addition, because the initial $^3P^o_0$ population is smaller in Fig. 5 ($^3P^o_1$ depleted) than in Fig. 4 ($^3P^o_2$ depleted), the repopulation of the depleted level is less sensitive to the reverse $0\to1$ rate in Fig. 5 than it is to the $0\to2$ rate in Fig. 6. Both of these transfer processes are masked by the sizable $2\rightleftarrows1$ rates and the large initial $^3P^o_2$ populations.

It should be noted that the inelastic cross sections reported in Table I include all encounters in which $Ca(^3P^o_J)$

TABLE I. Derived velocity-averaged cross sections (in Å^2) for collisions of $Ca(^3P^o)$ with He.[a]

Process	$\bar{\sigma}$ Present experimental results[b]	$\bar{\sigma}$ Theoretical calculation[c]
Elastic attenuation		
σ_e	42.9±7.3	
Intramultiplet mixing		
$\sigma_{2\to1}$	31.9±4.2	11.2
$\sigma_{2\to0}$	5.5±1.6	0.8
$\sigma_{1\to0}$	2.0±5.0	2.5

[a]Average collision energy 0.0556 ± 0.0015 eV.
[b]Uncertainties given as ± one standard deviation.
[c]Reference 27.

atoms are inelastically scattered forward in the laboratory frame into the laser detection zone. Thus, these cross sections are, strictly speaking, lower limits to the integral cross sections, although the laser detection zone was made as large as possible to allow detection of atoms scattered to large laboratory angles. We are fortunate in this system that the small mass of the helium target causes a kinematic compression of center of mass (c.m.) scattering angles in the laboratory frame. Unpublished calculations[48] at 0.05, 0.14, and 0.30 eV collision energy also indicate that the inelastic c.m. differential cross sections 0.14 eV and above are forward peaked. Finally, the apparatus-effective elastic cross section reported in Table I is a small fraction of the calculated[48] elastic integral cross sections, which are approximately 280 Å^2.

V. DISCUSSION

By the use of an optical-pumping state-selection technique, it has been possible to determine the rate constants for intramultiplet transfer between the Ca($^3P_J^o$) spin-orbit levels in collisions with helium. Previous work on collisional intramultiplet mixing in ^3P states has involved the heavy-atom systems Hg and Cd, where the spin-orbit splittings are much larger, and mainly the $^3P_1 \rightarrow {}^3P_0$ transfer rate has been studied[10–13,16,18] in cell experiments. There have also been two crossed beam studies[14,15] in which the velocity dependence of $^3P_2 \rightarrow {}^3P_1$ transfer in Hg has been determined. The most complete previous work on intramultiplet mixing in a ^3P state is a recent study of Breckenridge and Malmin,[17] who estimated Cd(^3P_J)-hydrocarbon mixing rate constants from the observed collisional equilibration of the ^3P_J populations after quenching of the Cd(^1P) level. Unfortunately, the estimation of the intramultiplet mixing rates was hampered by the concomitant translational relaxation of the ^3P_J atoms.

Because the collision energy is considerably greater than the Ca($^3P^o$) fine-structure spacings, the simplest model with which to compare our results is a statistical theory,[49] in which the cross sections $\sigma_{J\rightarrow J'}$ would be expected to be proportional to the final-state degeneracy $(2J'+1)$. Thus, the ratio of the $2\rightarrow1$ to $2\rightarrow0$ cross sections are predicted to be $\frac{5}{3}=1.67$. From Table I, the experimental ratio is found to be considerably greater (5.8 ± 1.7).

In the accompanying paper, Alexander, Orlikowski, and Straub[27] have computed intramultiplet mixing cross sections for Ca($^3P_J^o$)-He collisions [Eq. (1)] as a function of relative energy. A quantum close-coupling (CC) treatment using CaHe $^3\Pi$ and $^3\Sigma$ potential energy curves derived by a pseudopotential calculation[28] was employed. Cross sections were also obtained with a j_z-conserving (coupled states) simplification, but these were found to agree poorly with the CC results.

Alexander *et al.*[27] find that the CC cross sections for Ca($^3P_J^o$)-He collisions vary significantly (see Fig. 3 of Ref. 27) over the broad translational energy distribution (Fig. 7) in our beam-gas experiment. Accordingly, to facilitate comparison of theory and experiment, our cross sections $\bar{\sigma}$ are compared with calculated cross sections which have been averaged over our experimental relative energy distribution $f(E)$[27]:

$$\bar{\sigma}_{J\rightarrow J'}=\int \sigma_{J\rightarrow J'}(E)E^{1/2}f(E)dE \Big/ \int E^{1/2}f(E)dE \ . \quad (6)$$

The resulting theoretical cross sections $\bar{\sigma}$ are displayed in Table I.

In both the theoretical and experimental results, the largest cross section is found to be for the $2\rightarrow1$ transition. However, the agreement of the magnitudes of the cross sections is poor, worse than the comparison between the experimental intramultiplet rate constants[50] and CC cross sections[51] for the Na($^2P^o$)-He system. The latter quantities were calculated using the pseudopotential curves of Baylis.[52] Malvern[28] employed an analogous pseudopotential method to obtain the Ca($^3P^o$)-He curves. The present experimental values of the Ca($^3P^o$)-He $2\rightarrow1$ and $2\rightarrow0$ cross section are three to four times larger than the calculated theoretical values of Alexander *et al.*[27]

Theory and experiment also differ in the ratio of the $1\rightarrow0$ and $2\rightarrow0$ cross sections. The former predicts that the $1\rightarrow0$ cross section should be the larger of the two, while our experiments indicate that the $2\rightarrow0$ cross sections are approximately three times larger than the $1\rightarrow0$ cross section. Although the $1\rightarrow0$ cross section is not determined well by these experiments, nevertheless it does appear to have significant magnitude. The theoretical calculations predict an appreciable $1\rightarrow0$ cross section even though there is no electrostatic coupling between the $J=0$ and 1 levels.[27] This $1\rightarrow0$ transfer occurs because of coriolis coupling between the orbital and electronic angular momenta. It is interesting to note that the $1\rightarrow0$ cross sections in Hg and Cd are found to be very small,[10–13,16–17] suggesting that coriolis coupling cannot facilitate this mixing in ^3P states where the spin-orbit coupling is much larger than the translational energy.[53]

Several improvements in this experiment would be desirable to make the comparison of theory and experiment more incisive. Implementation of a crossed beam geometry would allow a reduction in the spread of translational energies, as well as a probing of the energy dependence of the three intramultiplet cross sections. Preparation of a single initial $^3P_J^o$ spin-orbit level would also be helpful in simplifying the extraction of cross sections from the experimental data. This is most easily achieved with the $^3P_1^o$ level, which can be excited with the $^3P_1^o \leftarrow {}^1S$ intercombination line. Finally, it should be noted that the potential-energy curves used in the theoretical computations[27] were derived from a pseudopotential calculation[27] which explicitly included only the two Ca valence electrons. Hopefully, the disagreements between theory and experiment will be reduced if the $^3\Pi$ and $^3\Sigma$ curves were obtained from an all-electron *ab initio* computation. Theoretical studies[51,54] on the Na($^2P^o$)-He system have shown that intramultiplet cross sections are very sensitive to the assumed potential energy curves, at least for that system.

In this paper, we have presented an optical-pumping state-selection technique for studying collisions of ^3P atoms in individual spin-orbit states. This technique has been used to determine intramultiplet mixing cross sections in the Ca($^3P^o$)-He system. Because of the presence of three possible fine-structure-changing transitions, ^3P atoms possess a richness and complexity not found in the analogous collisional process in ^2P states. It will be very interesting to extend these studies to other rare-gas targets and to molecular species.

ACKNOWLEDGMENTS

We are grateful to our theorist collaborators, Millard Alexander and Tadeusz Orlikowski, for numerous stimulating discussions and for their insight on the interpretation of our experimental results. We also acknowledge S. D. Rosner for a discussion on optical pumping and for providing us with a copy of Ref. 37 prior to publication. This work was supported by the National Science Foundation under Grant No. CHE-81-08464, by the U. S. Army Research Office under Grant No. DAAG29-81-K-0102, and by the North Atlantic Treaty Organization under Travel Grant No. 232.81. One of us (P.J.D.) would like to acknowledge a teacher-scholar grant from the Camille and Henry Dreyfus Foundation.

APPENDIX A: DENSITY-MATRIX CALCULATION OF THE OPTICAL-PUMPING STATE-SELECTION PROCESS

We present here a calculation of the optical-pumping process, which demonstrates that no coherences are generated. In addition, the M_J distributions are found to be nearly isotropic.

We employ a density-matrix formalism with a basis set including all the M_J levels of the $^3P_J^o$ and $^3S_1$ states (12 M_J levels in all). All unique, nonzero elements of this 12×12 density matrix were thus considered. The rate of change of the density matrix is governed by the Liouville equation[36]:

$$\frac{\partial\rho}{\partial t}=\frac{1}{i\hbar}[H_o,\rho]+L(\rho)\ , \tag{A1}$$

where H_o is the Hamiltonian in the absence of all external fields and $L(\rho)$ includes the interaction with the laser field (absorption and stimulated emission), spontaneous radiative decay, and the effects of the earth's magnetic field. In the present calculation, Eq. (A1) was transformed into the interaction picture [Eq. (II.2) of Ref. 36]:

$$\frac{d\tilde{\rho}}{dt}=\tilde{L}(\rho)\ . \tag{A2}$$

In $\tilde{L}(\rho)$, the terms describing spontaneous radiative decay are taken from Eq. (4) of Ref. 37:

$$\frac{d\tilde{\rho}_e}{dt}=-\Gamma\tilde{\rho}_e\ , \tag{A3a}$$

$$\frac{d\tilde{\rho}_{eg}}{dt}=-\frac{\Gamma}{2}\tilde{\rho}_{eg}\ , \tag{A3b}$$

$$\frac{d\tilde{\rho}_g}{dt}=\psi(\tilde{\rho}_e)\ . \tag{A3c}$$

Here $\tilde{\rho}_e$ and $\tilde{\rho}_g$ are the excited $^3S_1$ and ground $^3P_J^o$ density matrices, respectively; and $\tilde{\rho}_{eg}$ represents the coherence between ground and excited states. The spontaneous radiative decay rate of the excited states is denoted by Γ, and $\psi(\tilde{\rho}_e)$ is given by Eq. (III.81) of Ref. 36. The remaining terms in $\tilde{L}(\rho)$ are given by $(1/ih)[\tilde{H}_{\rm opt},\tilde{\rho}]$ and $(1/ih)[\tilde{H}_{\rm mag},\tilde{\rho}]$. The first term represents the interaction with the laser field and is given by

$$\langle e\,|\,\tilde{H}_{\rm opt}\,|\,g\rangle=-\langle e\,|\,\vec{\rm P}\,|\,g\rangle\cdot\vec{\rm E}\ , \tag{A4}$$

where $\langle e\,|\,\vec{\rm P}\,|\,g\rangle$ is a matrix element of the electric dipole operator and $\vec{\rm E}$ is the electric field amplitude of the laser (assumed to be monochromatic). Finally, $\tilde{H}_{\rm mag}$ describes the interaction with the earth's magnetic field. The $^3S_1\rightarrow{}^3P_J^o$ radiative transition possibilities and dipole matrix elements were obtained from the compilation of Wiese *et al.*[55]

In our experimental arrangement, the atomic beam direction, cw laser polarization, and the earth's magnetic field were approximately mutually perpendicular. In our numerical integration of Eq. (A2), the coordinate axes were defined so that these directions were along the y, x, and z axes, respectively. The initial populations at the optical-pumping region ($^3P_2^o$:$^3P_1^o$:$^3P_0^o$=1:0.391:0.156) were obtained by laser fluorescence measurements with the pulsed dye laser in the scattering chamber and corrected for $^3P_1^o\rightarrow{}^1S$ radiative decay. The cw laser power density and the earth's magnetic field strength were taken to be 50 mW/cm^2 and 0.5 G,[56] respectively.

We find that after irradiation for 3 μsec, any pumped $^3P_J^o$ level is essentially completely depleted. The time required for depletion is smallest for $^3P_0^o$ and largest for $^3P_2^o$; it should be noted that the average irradiation time in our experiment is 9.5 μsec. One function of the earth's magnetic field is to mix the M_J levels and hence allow all atoms to be pumped. During free flight to the scattering chamber (190 μsec, on average), the off-diagonal elements of the interaction-picture density matrix oscillate because of the earth's magnetic field (Larmor frequency 1.1 MHz). These off-diagonal elements average to zero when the dispersion in flight times due to the Ca($^3P^o$) velocity distribution is taken into account. Thus, there are no coherences generated in the unpumped $^3P_J^o$ states by our optical-pumping state-selection technique.

Table II presents the predicted (J,M_J) populations when each $^3P_J^o$ state is optically pumped; the z quantization axis has been brought into coincidence with the incident atomic beam direction, the unique axis in the scattering experiment. It can be seen that the M_J distributions in the unpumped $^3P_J^o$ states are calculated to be slightly anisotropic. While the present calculation may not strictly apply to our experiment, it nevertheless indicates that the true M_J distributions are not highly anisotropic.

In Appendix B, we consider the effect of these anisotropic distributions on the fluorescence intensity factors.[57] Table II can also be used to predict the enhancement in the unpumped $^3P_J^o$ populations when the pump laser is turned on. As can be seen from Table III, the experimentally observed enhancements are very close to the predicted values.

APPENDIX B: INTENSITY FACTORS FOR LASER FLUORESCENCE DETECTION OF THE $^3S_1\rightarrow{}^3P_J^o$ MULTIPLET

In our detection scheme, a Ca $^3P_J^o$ level is laser excited to the $^3S_1$ level, and the resulting fluorescence back to the $^3P_J^o$ multiplet is detected. We follow the notation in our earlier treatments[57,58] of intensity factors and denote the total angular momentum of the Ca $^3P_J^o$ atoms to be detected as $j_2(=J)$; for the excited $^3S_1$ state, we have $j_3=1$. In the notation of Refs. 57 and 58, the fluorescence intensity following excitation of the $^3S_1\leftarrow{}^3P_J^o$ by radiation linearly

TABLE II. Predicted $^3P_J^o$ populations under cw laser pumping of individual lines in the $^3S_1 \leftarrow {}^3P_J^o$ multiplet.[a]

Pumped $^3P_J^o$ level	Irradiation time (μsec)	J	M_J[b]	Population[c]
$^3P_0^o$	0.5	0	0	<0.0001
		1	±1	0.0984
		1	0	0.0936
		2	±2	0.1387
		2	±1	0.1434
		2	0	0.1450
$^3P_1^o$	2	0	0	0.1428
		1	$0,\pm1$	<0.0001
		2	±2	0.1839
		2	±1	0.1650
		2	0	0.1587
$^3P_2^o$	3	0	0	0.2621
		1	±1	0.2396
		1	0	0.2540
		2	$0,\pm1,\pm2$	<0.0001

[a]The initial populations of the individual M_J states, obtained from laser fluorescence measurements, are given by 0.1293, 0.0843, and 0.1008 for the $^3P_2^o$, $^3P_1^o$, and $^3P_0^o$ levels, respectively, the M_J distribution in each $^3P_J^o$ level was assumed isotropic. The pump laser density and the earth's magnetic field were 50 mW/cm^2 and 0.5 G, respectively.
[b]Quantization axis along the incident atomic beam direction.
[c]Total population normalized to unity.

polarized in the x_i direction is given by

$$I_{j_2,j_3}(x_i)=\sum_{\mu_2,x_j,j_4} N_{j_2\mu_2} I_{j_2\mu_2,j_3j_4}(x_i,x_j)\ . \tag{B1}$$

Here, $I_{j_2\mu_2,j_3j_4}(x_i,x_j)$ is given by Eq. (46) of Ref. 57 and represents the $j_3 \rightarrow j_4$ x_j-polarized fluorescence following x_i-polarized laser excitation of atoms in the $j_2\mu_2$ state to the j_3 level. The populations of the magnetic sublevels are denoted as $N_{j_2\mu_2}$, and their sum is normalized to unity. Equation (B1) is valid for the present experiment since no coherences are present (see Appendix A) and hyperfine splittings are absent.

We choose the z axis to be the atomic beam direction; Fig. 1 of Ref. 57 shows the arrangement of the laser and photodetector. The fluorescence polarization is not resolved so that the sum over x_j is over the y and z axes. If we assume the μ_2 distribution is isotropic, i.e., $N_{j_2\mu_2}=(2j_2+1)^{-1}$, then the fluorescence intensity [Eq. (B1)], after some algebra,[59] is found to be independent of the laser polarization and the j_2 quantum number:

$$I_{j_2,j_3}(z)=I_{j_2,j_3}(x)=\tfrac{2}{3}(2j_3+1)^2(-1)^{j_2}$$
$$\times \begin{Bmatrix} 0 & j_3 & 1 \\ j_2 & 1 & 1 \end{Bmatrix} \begin{Bmatrix} 1 & j_2 & 1 \\ j_3 & 0 & 1 \end{Bmatrix} \sum_{j_4} (2j_4+1)(-1)^{j_4} \begin{Bmatrix} 0 & j_3 & 1 \\ j_4 & 1 & 1 \end{Bmatrix} \begin{Bmatrix} 1 & j_4 & 1 \\ j_3 & 0 & 1 \end{Bmatrix} \begin{Bmatrix} j_3 & j_3 & 0 \\ 1 & 1 & j_4 \end{Bmatrix} \begin{Bmatrix} j_3 & j_3 & 0 \\ 1 & 1 & j_2 \end{Bmatrix} = \frac{2}{27}\ . \tag{B2}$$

TABLE III. Increase in the $^3P_J^o$ fluorescence signals when the cw dye laser optically pumps another spin-orbit level.

Pumped $^3P_J^o$ level	Detected $^3P_J^o$ level	Increase in fluorescence with pumping Observed	Calculated[a]
$^3P_0^o$	$^3P_1^o$	1.21 ± 0.04	1.141
	$^3P_2^o$	1.11 ± 0.06	1.091
$^3P_1^o$	$^3P_0^o$	1.49 ± 0.06	1.417
	$^3P_2^o$	1.48 ± 0.12	1.349
$^3P_2^o$	$^3P_0^o$	2.92 ± 0.29	2.600
	$^3P_1^o$	3.06 ± 0.09	2.920

[a]Obtained from the optical-pumping calculation in Table II and the fluorescence intensity factors in Table IV.

TABLE IV. Calculated $^3S_1 \leftarrow {}^3P_J^o$ fluorescence intensity factors for various assumed μ_2 distributions.[a]

Pumped $^3P_J^o$ level	Detected $^3P_J^o$ [b] level	Assumed μ_2 distribution	
		Isotropic	Anisotropic[c]
0	0	0.021 00	
	1	0.023 51	0.023 36
	2	0.022 50	0.022 38
1	0	0.021 00	0.021 00
	1	0.023 51	
	2	0.022 50	0.022 91
2	0	0.021 00	0.021 00
	1	0.023 51	0.023 67
	2	0.022 50	

[a]The excitation and detection conditions apply to our experimental arrangement: laser polarization $P=82.3\%$; filter transmission 0.5, 2.5, and 53.5 % at the $J=0,1,2$ lines, respectively, of the $^3S_1 \rightarrow {}^3P_J^o$ multiplet.

[b]Total population in each $^3P_J^o$ level normalized to unity, i.e., $\sum_{\mu_2} N_{j_2\mu_2}=1$.

[c]The μ_2 distribution given by the optical-pumping calculation in Appendix A (see Table II).

It is interesting to note that straightforward use of the line-strength factors S_{j_2,j_3} defined by Condon and Shortley,[60] which are appropriate only for isotropic irradiation and detection, also predict that the spectral intensity I_{j_2,j_3} is directly proportional to the total $^3P_J^o$ population $N_{j_2}=\sum_{\mu_2} N_{j_2\mu_2}$:

$$I_{j_2,j_3}=N_{j_2}S_{j_2,j_3}/(2j_2+1)\ , \tag{B3}$$

since S_{j_2,j_3} is proportional to $(2j_2+1)/3$ for a $^3S_1 \leftarrow {}^3P_J^o$ multiplet.[61]

In our actual experiment setup, Eq. (B1) does not exactly apply since the 10-nm FWHM filter in front of the fluorescence detector did not transmit equally the three $j_3 \rightarrow j_4$ fluorescence lines. In addition, the incident (and possibly scattered) $^3P_J^o$ levels were calculated in Appendix A to be slightly anistropic because of the optical-pumping process. Finally, the detector dye laser is not completely polarized, but has polarization $P=(I_x-I_z)/(I_x+I_z)=82.3\%$. A suitably modified form of Eq. (B1) was used to calculate fluorescence intensity factors for the two limiting cases of an isotropic μ_2 distribution and the distributions calculated in Appendix A, and the results are presented in Table IV. It can be seen that the calculated factors differ only insignificantly for these two cases. This suggests that the factors for the actual μ_2 distributions present in our experiments should be very close to those calculated for an isotropic distribution. We have employed those factors assuming an isotropic μ_2 distribution in relating experimental fluorescence intensities to populations.

[1]L. Krause, Adv. Chem. Phys. 28, 267 (1975); E. E. Nikitin, *ibid.* 28, 317 (1975), and references therein.

[2]R. W. Anderson, T. P. Goddard, C. Parravano, and J. Warner, J. Chem. Phys. 64, 4037 (1976).

[3]J. Apt and D. E. Pritchard, J. Phys. B 12, 83 (1979).

[4]J. M. Mestdagh, J. Cuvellier, J. Berlande, A. Binet, and P. dePujo, J. Phys. B 13, 4589 (1980); J. M. Mestdagh, J. Berlande, J. Cuvellier, P. dePujo, and A. Binet, *ibid.* 15, 439 (1982); J. M. Mestdagh, P. dePujo, J. Cuvellier, A. Binet, P. R. Fournier, and J. Berlande, *ibid.* 15, 663 (1982).

[5]J. Elward-Berry and M. J. Berry, J. Chem. Phys. 72, 4500 (1980).

[6]R. Boggy and F. A. Franz, Phys. Rev. A 25, 1887 (1982).

[7]R. A. Phaneuf and L. Krause, Can. J. Phys. 58, 1047 (1980); I. N. Siara, R. U. Dubois, and L. Krause, *ibid.* 60, 239 (1982).

[8]B. Amaee and C. Bottcher, J. Phys. B 11, 1249 (1978); P. Habitz, Chem. Phys. 54, 131 (1980).

[9]A. P. Hickman, Phys. Rev. Lett. 47, 1585 (1981).

[10]J. S. Deech, J. Pitre, and L. Krause, Can. J. Phys. 49, 1976 (1971).

[11]W. H. Breckenridge, T. W. Broadbent, and D. S. Moore, J. Phys. Chem. 79, 1233 (1975).

[12]A. C. Vikis, G. Tome, and D. J. LeRoy, Can. J. Chem. 50, 176 (1972).

[13]H. Umemoto, S. Tsunashima, and S. Sato, Chem. Phys. 43, 93 (1979); 47, 257 (1980).

[14]H. F. Krause, S. Datz, and S. G. Johnson, J. Chem. Phys. 58, 367 (1973).

[15]K. Liu and J. M. Parson, J. Chem. Phys. 65, 815 (1976).

[16]J. Pitre, K. Hammond, and L. Krause, Phys. Rev. A 6, 2101 (1972).

[17]W. H. Breckenridge and O. K. Malmin, J. Chem. Phys. 76, 1812 (1982).

[18]M. Czajkowski, E. Walentynowicz, and L. Krause, J. Quant. Spectrosc. Radiat. Transfer 28, 13 (1982).

[19]S. A. Arbadji, D. Hennecart, and D. Lecler, J. Phys. (Paris) 43, 37 (1982).

[20]H. Honguchi and S. Tsuchiya, Bull. Chem. Soc. Jpn. 50, 1661 (1977).

[21]P. D. Foo, J. R. Wiesenfeld, M. J. Yuen, and D. Husain, J. Phys. Chem. 80, 91 (1976).

[22]W. H. Breckenridge and A. M. Renlund, J. Phys. Chem. 83, 303 (1979).

[23]M. A. Chowdhury and D. Husain, J. Photochem. 10, 277 (1979).

[24]P. S. Furcinitti, J. J. Wright, and L. C. Balling, Phys. Rev. A

12, 1123 (1975).
[25]P. S. Furcinitti, L. C. Balling, and J. J. Wright, Phys. Lett. 53A, 75 (1975); P. G. Whitkop and J. R. Wiesenfeld, Chem. Phys. Lett. 69, 457 (1980).
[26]M. D. Havey, L. C. Balling, and J. J. Wright, Phys. Rev. A 13, 1269 (1976).
[27]M. H. Alexander, T. Orlikowski, and J. E. Straub, following paper, Phys. Rev. A 28, 73 (1983).
[28]A. R. Malvern, J. Phys. B 11, 831 (1978).
[29]S. D. Rosner, R. A. Holt, and T. D. Gaily, Phys. Rev. Lett. 35, 785 (1975); S. D. Rosner, T. D. Gaily, and R. A. Holt, *ibid.* 40, 851 (1978).
[30]W. Ertmer and B. Hofer, Z. Phys. A 276, 9 (1976).
[31]W. J. Childs, O. Poulson, and L. S. Goodman, Phys. Rev. A 19, 160 (1979).
[32]K. Bergmann, R. Engelhardt, U. Hefter, and J. Witt, J. Phys. E 12, 507 (1979).
[33]J. A. Irvin and P. J. Dagdigian, J. Chem. Phys. 73, 176 (1980); 74, 6178 (1981).
[34]J. L. Hall and S. A. Lee, Appl. Phys. Lett. 29, 367 (1976).
[35]P. J. Dagdigian, J. Chem. Phys. 76, 5375 (1982).
[36]W. Happer, Rev. Mod. Phys. 44, 169 (1972).
[37]C. Cohen-Tannoudji, in *Atomic Physics 4,* edited by G. zu-Putlitz, E. W. Weber, and A. Winnacker (Plenum, New York, 1979), pp. 589—614.
[38]A. G. Adam, S. D. Rosner, T. D. Gaily, and R. A. Holt, Phys. Rev. A 26, 315 (1982).
[39]R. J. Malins and D. J. Benard, Chem. Phys. Lett. 74, 321 (1980).
[40]I. W. M. Smith, *Kinetics and Dynamics of Elementary Gas Reactions* (Butterworths, London, 1980).
[41]R. N. Diffenderfer, P. J. Dagdigian, and D. R. Yarkony, J. Phys. B 14, 21 (1981).
[42]L. Pasternack, D. M. Silver, D. R. Yarkony, and P. J. Dagdigian, J. Phys. B 13, 2231 (1980).
[43]G. Guisfredi, P. Minguzzi, F. Strumia, and M. Tonelli, Z. Phys. A 274, 279 (1975).
[44]M. Abramowitz and I. Stegun, *Handbook of Mathematical Functions,* Appl. Math. Series 55 (National Bureau of Standards, Washington, D.C., 1965).
[45]L. Pasternack and P. J. Dagdigian, J. Chem. Phys. 67, 3854 (1977).
[46]R. C. Estler and R. N. Zare, Chem. Phys. 28, 253 (1978).
[47]P. R. Bevington, *Data Reduction and Error Analysis for the Physical Sciences* (McGraw-Hill, New York, 1969).
[48]T. Orlikowski and M. H. Alexander, unpublished results.
[49]See, for example, R. D. Levine, R. B. Bernstein, P. Kahana, I. Procaccia, and E. T. Upchurch, J. Chem. Phys. 64, 5661 (1977).
[50]J. A. Jordan and P. A. Franken, Phys. Rev. 142, 20 (1966); J. Pitre and L. Krause, Can. J. Phys. 45, 2671 (1967).
[51]R. H. G. Reid, J. Phys. B 6, 2018 (1973).
[52]W. E. Baylis, J. Chem. Phys. 51, 2665 (1969).
[53]A. I. Voronin and V. A. Kvlividze, Theor. Chim. Acta 8, 334 (1967).
[54]A. D. Wilson and Y. Shimoni, J. Phys. B 7, 1543 (1974); 8, 1392, (1975); 8, 2393 (1975).
[55]W. L. Wiese, M. W. Smith, and B. M. Miles, Natl. Bur. Stand. Ref. Data Ser. 22, Vol. III (1969).
[56]*American Institute of Physics Handbook,* 3rd ed. (McGraw-Hill, New York, 1972).
[57]M. H. Alexander, P. J. Dagdigian, and A. E. DePristo, J. Chem. Phys. 66, 59 (1977).
[58]P. J. Dagdigian, B. E. Wilcomb, and M. H. Alexander, J. Chem. Phys. 71, 1670 (1979).
[59]Compare the Appendix of Ref. 57 and A. P. Yutsis, I. B. Levinson, and V. V. Vanagas, *The Theory of Angular Momentum,* translated by A. Sen and R. N. Sen (Israel Program for Scientific Translations, Jerusalem, 1962).
[60]E. U. Condon and G. H. Shortley, *The Theory of Atomic Spectra* (Cambridge University Press, Cambridge, England, 1935).
[61]A. R. Edmonds, *Angular Momentum in Quantum Mechanics* (Princeton University Press, Princeton, N.J., 1960).